5th Australasian Congress on Applied Mechanics, ACAM 2007
10-12 December 2007, Brisbane, Australia

SAW driven microchannel flow

M. K. Tan[1], J. R. Friend, and L. Y. Yeo

[1]*Department of Mechanical Engineering, Monash University, Australia*

In this paper a new method for surface acoustic wave (SAW) driven microchannel flow is introduced. This method employs a laser ablation system to create a groove type microchannel on the 128^0 rotated Y-cut X-propagating Lithium Niobate ($LiNbO_3$, LN), to provide two walls as the driving source that radiate acoustic energy into the fluid. This new configuration allows the fluid to flow in the microchannel without generate vortices for a channel width less than 50 μm at a driving frequency of 30 MHz. Numerical analysis was performed and the results agreed with the experimental findings. The potential application of this new configuration for SAW driven microchannel flow is to propel fluid in *Lab-on-a-chip* devices.

Keywords: acoustic streaming, surface acoustic wave.

1 Introduction

The direct generation surface acoustic wave on a piezoelectric substrate using interdigital electrodes was first reported by White and Volter [1]. The devices were fabricated using photolithography technique to produce an interdigital pattern on a metallic coating that sputtered on the piezoelectric substrate. Acoustic wave was generated along the surface of the piezoelectric substrate by applying a high-frequency signal to the interdigital transducer (IDT). If the substrate consists of Y-cut, X-propagating $LiNbO_3$, Rayleigh waves can be generated. Upon placing a water droplet upon the surface of the substrate to interact with the surface acoustic wave (SAW), the axially-polarized compressional displacement component is diffracted at the Rayleigh angle into the droplet, generating so-called Leaky SAW [2]. The leaky component of the SAW induces an acoustic pressure gradient inside the droplet, giving rise to acoustic streaming. For high-power ultrasonic excitation, the induced streaming motion imparts inertia to the fluid, giving rise to acoustic steaming jets [3] or atomization [4], below which the droplet vibrates and translates along the direction of the SAW propagation [5-7], Figure 1.

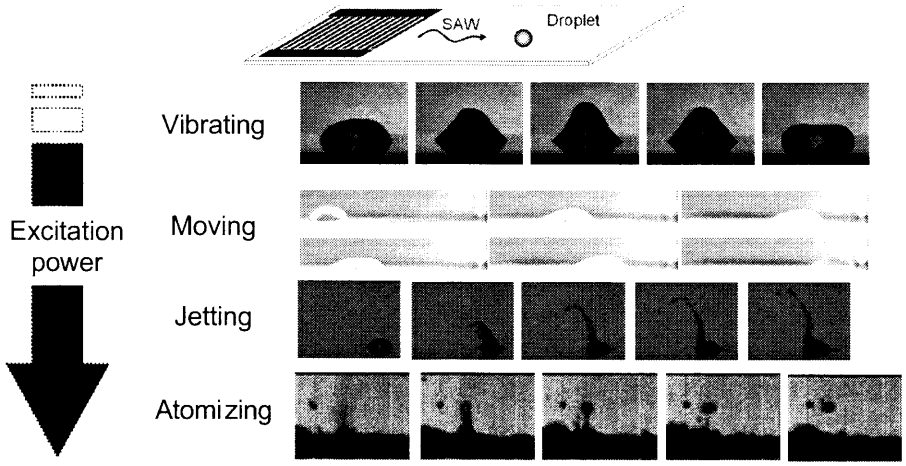

FIG. 1: Droplet behaviour with increasing excitation power.

Tseng *et al* [8] and Sritharan *et al* [9] extended this SAW-streaming actuation mechanism from the free surface droplet manipulation to the enclosed microchannel flow, particularly for the micro-mixing application. In Tseng's experiment [8], the micro-mixer used a 9.6 MHz SAW device. The channels were fabricated directly on top of the substrate forming the single radiator configuration. Their microchannel was 200 μm wide and 100 μm high. Flow circulations were observed in the channel and the fluid mixing was greatly enhanced when the channel was oriented transversely to the SAW direction. On the other hand, Sritharan [9] placed a 146 MHz SAW device directly underneath a substrate which had a microchannel fabricated on, to form a hybrid system. The channel was 75 μm wide and 100 μm high. Similarly, the SAW device was oriented such that the surface waves propagate

transversely to the flow direction to induce vortex-flow in the channel. Vortexes are critical for micro-mixing application but it hinder the SAW-actuation for microchannel pump application. Vortex causes the local flow circulation and thus results in the low net flow through the channel. In this paper, we propose a new configuration that enables the SAW induced microchannel flow without vortices. By utilizing the configuration of SAW propagates in parallel to the fluid flow direction, together with the propose dual-radiators configuration, the formation of vortices is suppressed. This straight flow is highly desirable for the micropumps application.

2 Numerical analysis

A Cartesian coordinate system x_i (i =1, 2, 3) is chosen with x_3 defining the transverse direction, and x_1 defining the direction of wave propagation. Consider a fluid-solid half-space system as shown in Fig. 2(a), the solid half-space is given by $x_3 > 0$, and the fluid by $x_3 < 0$. The partial differential equations governed the displacement and electric field potential in the piezoelectric crystal are [10, 11]:

$$C_{ijkl}\xi_{k,li} + e_{kij}\varphi_{,ki} = \rho_s \frac{\partial^2 \xi_j}{\partial t^2} \tag{1}$$

$$e_{ikl}\xi_{k,li} - \varepsilon_{ik}\varphi_{,ki} = 0 \tag{2}$$

where ρ_s, $\varphi_{,ki}$, C_{ijkl}, e_{ikl}, ε_{ik}, and $\xi_{k,li}$ are the components of mass density, electrical potential, elastic stiffness constant, piezoelectric constant, dielectric constant, and mechanical displacement, respectively. An index preceded by a comma denotes differentiation with respect to a space coordinate, and the dot notation for differentiation with respect to time. In the crystal medium ($x_3 > 0$), the traveling wave has the solutions of the form [11]:

$$\xi_i = \beta_i \exp\left[-\alpha_s \omega x_3 / v_s\right] \exp\left[j\omega\left(t - x_1 / v_s\right)\right], \quad i = 1,2,3 \tag{3}$$

$$\varphi = \beta_4 \exp\left[-\alpha_s \omega x_3 / v_s\right] \exp\left[j\omega\left(t - x_1 / v_s\right)\right] \tag{4}$$

The solutions are then substituted into the differential equations (1) and (2), leading to a linear homogeneous system of four equations. For the non-trivial solution to exist, the determinant of the coefficients must be zero. Upon obtaining the four appropriate values of α_s, the corresponding values of β_i can be found from each α_s. The coupled field in the crystal is expressed as the linear combination of the partial fields, equation (5) and (6). The amplitude coefficients $B^{(1)}$, $B^{(2)}$, $B^{(3)}$ and $B^{(4)}$ are determined by the solid-liquid boundary conditions [11].

$$\xi_i = \sum_{l=1}^{4} B^{(l)} \beta_i^{(l)} \exp\left[-\alpha_s^{(l)} \omega x_3 / v_s\right] \exp\left[j\omega\left(t - x_1 / v_s\right)\right], \quad i = 1,2,3 \tag{5}$$

$$\varphi = \sum_{l=1}^{4} B^{(l)} \beta_4^{(l)} \exp\left[-\alpha_s^{(l)} \omega x_3 / v_s\right] \exp\left[j\omega\left(t - x_1 / v_s\right)\right] \tag{6}$$

In the fluid medium ($x_3 < 0$), the equation of motion is described by:

$$\rho_f \frac{\partial \mathbf{u}}{\partial t} = -\nabla p + \left(\eta + \frac{4}{3}\mu\right)\nabla^2 \mathbf{u} - \mu \nabla \times \nabla \times \mathbf{u} \tag{7}$$

where ρ_f, η, μ is the fluid density, fluid bulk modulus, and fluid viscosity respectively. The above equation can be uniquely decomposed into a longitudinal part of $\mathbf{u}$, satisfied the condition $\nabla \times \mathbf{u}_l$,

and a transverse part of u_t, which satisfied the condition ∇u_t [12]. Thus, the first-order Navier-Stokes equation can be divided into two separate equations; one described acoustic wave propagation in which relates pressure to the longitudinal part of u, the other expressed shear viscous wave which gives the behavior of the transverse part of u. In the fluid medium, the decomposed particle displacement and electric potential have the form [11]:

$$\xi_i = \gamma_i \exp\left[-\alpha_f \omega x_3 / v_s\right] \exp\left[j\omega\left(t - x_1 / v_s\right)\right], \quad i = 1,2 \tag{8}$$

$$\varphi = C \exp\left[-\alpha_f \omega x_3 / v_s\right] \exp\left[j\omega\left(t - x_1 / v_s\right)\right] \tag{9}$$

and for the shear viscous wave, the transverse wave has velocity of the form [13]:

$$u_t = A \exp\left[j\omega t - \frac{(j-1)}{d_v} x_3\right] \tag{10}$$

where $d_v = \sqrt{(2\mu)/(\rho\omega)}$ is the viscous boundary layer thickness. The amplitude coefficient of A in equation (10) is determined by the boundary condition for velocity continuous across the interface at x_3 = 0, between the crystal and fluid shear viscous velocities. Substituting solutions for particle displacement and potential waveforms, equation (8) and (9), into the partial differential equation described the motion in fluid medium gives the equation for α_f in terms of the velocity v_s.

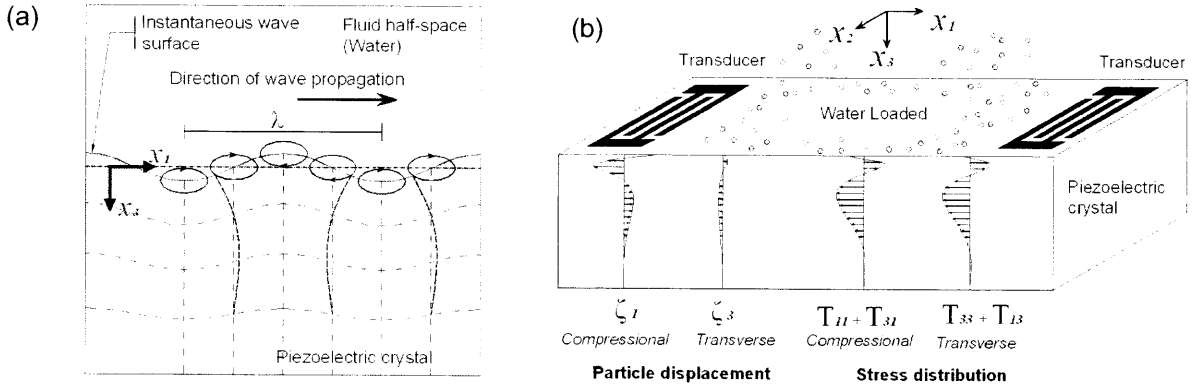

FIG. 2: SAW on the semi-infinite LN substrate coupled with the half-space water. (a) The motion of the solid particle elements of the LN substrate. (b) The displacement and stress distribution in the LN substrate when coupled with water.

The boundary conditions are employed to find the amplitude coefficients for the coupled-fields these are: continuity of fluid velocity at the interface between boundary layer and bulk fluid medium, continuity of electric potential at x_3 = 0 between solid and liquid, continuity of the normal component of electric displacement at x_3 = 0 between solid and liquid, continuity of normal stress component, and continuity of shear at x_3 = 0. Substituting the coupled field solutions (5), (6), (8), (9), and (10) to the boundary conditions to obtain the six homogeneous equations in the six unknown amplitude coefficients $B^{(1)}$, $B^{(2)}$, $B^{(3)}$, $B^{(4)}$, C, and γ_3. In order to obtain the surface wave velocity v_s, the determinant of the matrix coefficient must be zero for the nontrivial solution to exist.

The second-order system of equations for the fluid motion consists of the steady state and the time oscillating harmonic fields. Acoustic streaming is obtained from the time independent components of the fluid motion, thus the second-order time dependent terms have to be filtered out from the second-order system of equations by time averaging. This derives a pair of streaming equations as follow [12, 14]:

$$F_{dc} = -\frac{1}{c_0^2}\left\langle p_1 \frac{\partial u_1}{\partial t}\right\rangle - \rho_f \left\langle (u_1 \nabla) u_1 \right\rangle \tag{11}$$

$$F_{dc} = \nabla p_{dc} - \mu \nabla^2 u_{dc} - \left(\eta + \frac{1}{3}\mu \right) \nabla \nabla u_{dc} \qquad (12)$$

where F_{dc} is the body force density (N/m^3), p_{dc} is the second-order pressure, u_{dc} is the second-order streaming velocity, p_1 is the first-order acoustic pressure, and u_1 is the first-order acoustic velocity. The first-order fluid velocity field is obtained from the coupled-field equations between the piezoelectric crystal and the fluid and result is then substituted into equation (11) to get the body force distribution. Once the body force is obtained, equation (12) is solved for the streaming velocity, u_{dc}. For the free streaming case, channel with open ends, the differential of second-order pressure is assumed to be zero, $\nabla p_{dc} = 0$, and taking the assumption that the fluid is incompressible, $\nabla \cdot u_{dc} = 0$, equation (12) reduced to elliptical partial differential equation. Eq. (11) and (12) are then solved numerically using the finite-volume method.

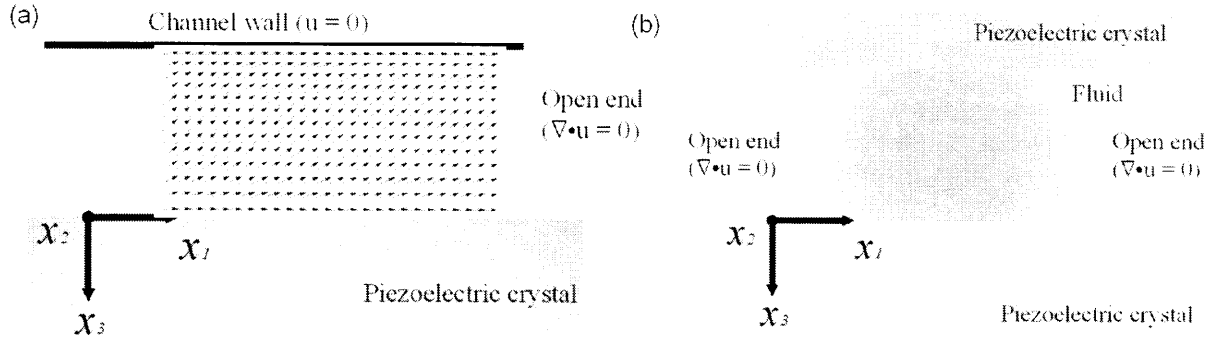

FIG. 2: The single and dual-radiator configuration for microchannel flow. (a) The channel builds on top of the LN substrate that provides a single wall as the radiator. Under the specified boundary conditions as labelled, the calculated flow field is showed in the inset. (b) The propose configuration provides two radiators. This configuration is achievable experimentally using laser ablation technique to create the groove type channel on the LN substrate.

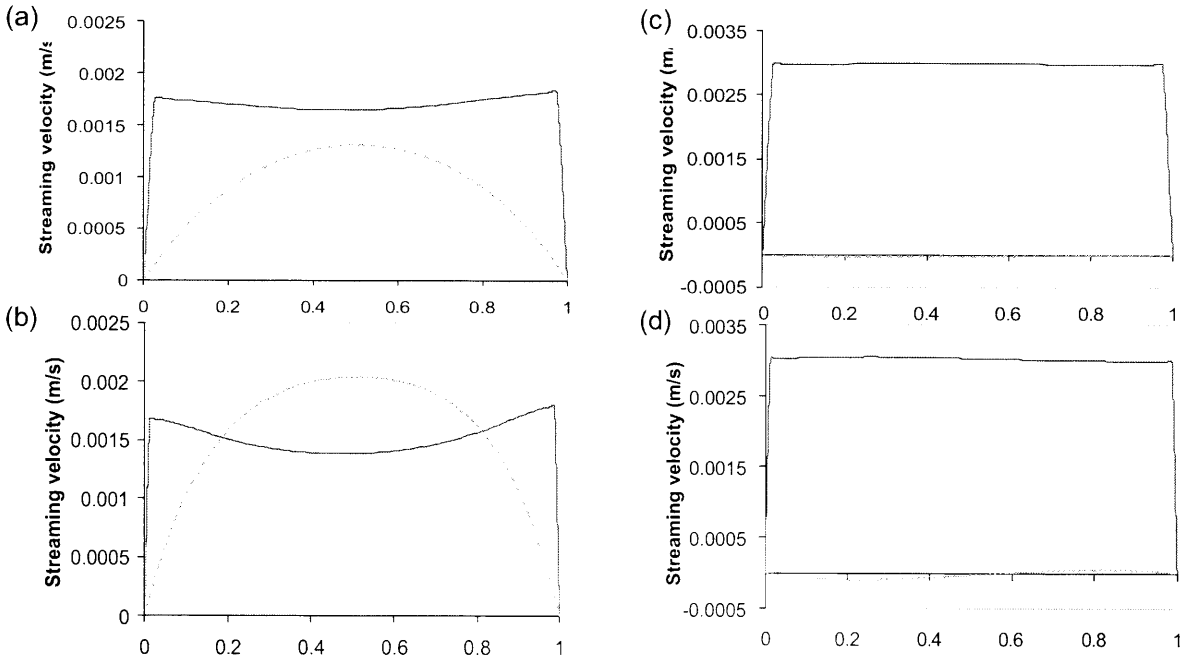

FIG. 3: Profiles of the x_1 (solid line) and x_3 (dashed line) components of the streaming velocity for travelling SAW in channels with different widths. (a) and (b) show the profiles for the single radiator configuration for channels of width 50 μm and 100 μm respectively. (c) and (d) show the profiles for the dual-radiator configuration for channels of width 50 μm and 100 μm, respectively.

Fig. 2(a) shows the velocity vector plot for streaming flow in microchannel. In the numerical analysis, no slip boundaries condition was assumed on the walls surface. Results indicate that the dominant actuation mechanism for acoustic streaming using a 128^0 Y-X LN is due to the radiated acoustic energy into the fluid and that induces the second-order fluid motion. As the channel height increases, streaming velocities magnitude perpendicular to the radiator surface increase dramatically, gives rise to the development of vortices, agreed with the Tseng's experiment. The new configuration is depicted in Fig. 2(b). This method has two important factors to achieve fluid flow without vortices. Firstly, as the waves propagate at nearly equal amplitude along two parallel radiator surfaces that faced opposite to one another, the radiated acoustic energy along x_3 direction will tend to balance out if the channel width is sufficiently small. Secondly, the streaming flow along the x_1 direction enhances significantly for the two parallel aligned radiators configuration.

Fig. 3 shows the numerical results for the single radiator and the two radiators configuration. The calculation was based on the assumption that no reflection from the side walls and waves propagate on the two radiators have equal amplitude. Fig. 3(a) and 3(b) show the calculated flow profile for single radiator configuration for 50 μm wide and 100 μm wide channels. Results indicate that the net flow along the x_1-direction is possible only for a sufficiently narrow channel; u_3-velocities begin to exceed the u_1-velocities when the channel size increases and thus allowing the formation of vortices. In contrast, dual-radiator configuration suppresses the influence of u_3-velocities and permits a more constant flow velocities across the channel width along the x_1-direction for the 50 μm channel, Fig. 3(c). As the channel width increases, the u_3-velocities begin to develop and have magnitudes symmetric with respect to the center of the channel, Fig. 3(d). This suggests that as the channel width increase further, vortices would still be induced under this dual-radiator configuration.

3 Microchannel fabrication and preliminary experimental results

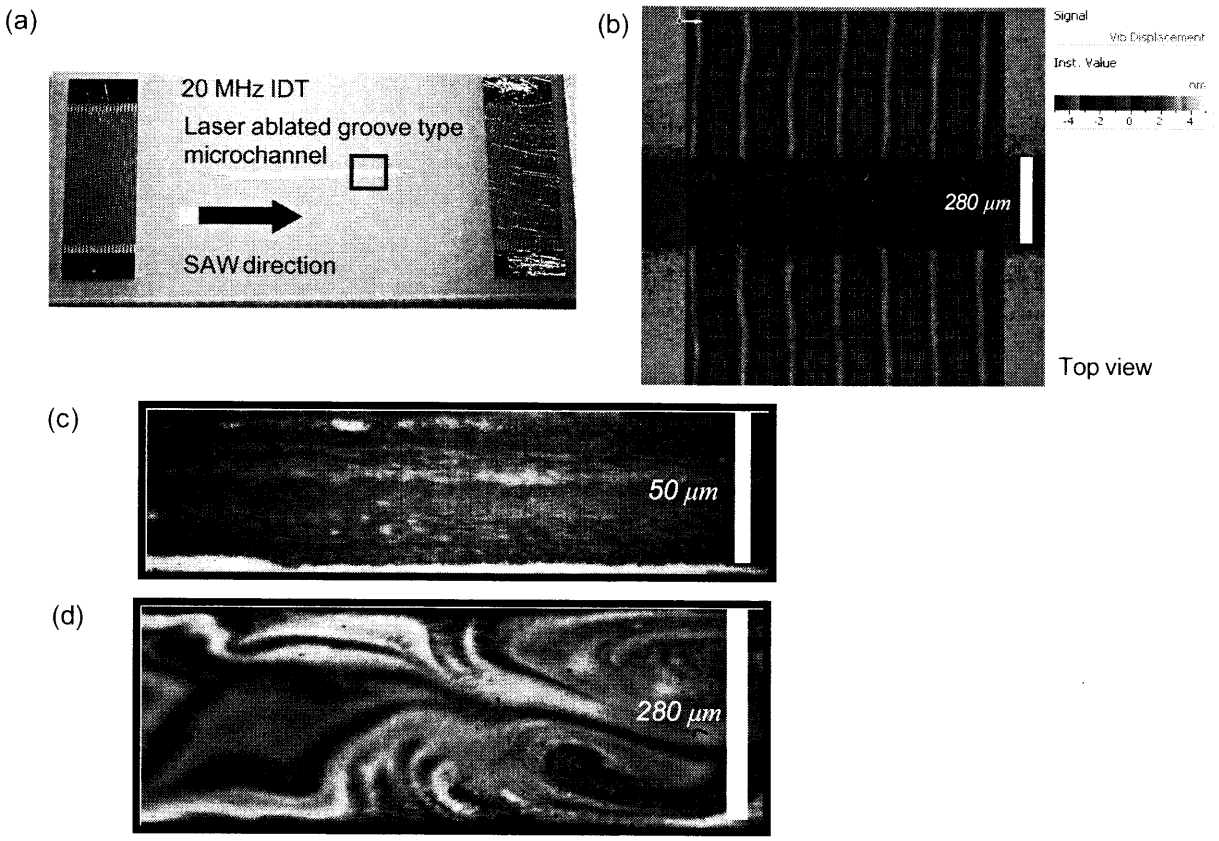

FIG. 4: (a) Laser ablated microchannel on a 20 MHz SAW device. (b) The measured instantaneous particle displacement amplitude on the LN substrate using laser doppler vibrometer. The result indicates that the channel walls were vibrating perpendicular to the SAW propagation direction, causes the distorted wavefront on the IN surface (indicated by the green lines). The flow visualization using fluorescent microparticles for streaming in the groove type microchannel of 50 μm wide channel (c), and 280 μm wide channel.

Preliminary experiments were carried out to verify the numerical findings for the groove type microchannel. The substrate was 128^0 rotated Y-cut X-propagating LN with thickness of 500 μm. A

pair of bidirectional interdigital transducer was fabricated on the substrate to launch the surface wave at 20 MHz frequency. The laser ablated microchannel has a rectangular cross section. Figure 4(a) shows the laser ablated channel on a 20 MHz SAW device. This channel was 280 μm in width, 200 μm in depth, and 10 mm in length. During the experiment, an absorbing material (α-gel, Geltec Ltd., Yokohama, Japan) was attached on the substrate edges to prevent wave reflection. Measuring the displacement perpendicular to the substrate surface with a scanning laser doppler vibrometer (MSA400, Polytec PI, Waldbrunn, Germany) showed that the vibration amplitudes were higher along the edges between the ablated regions than the substrate surface under the free boundaries condition, since there was no coverslip. The results also revealed that along these channel walls the vibration was essentially in 3-dimensions; the channel walls were vibrating at the direction perpendicular to the surface wave that propagates along the substrate surface. This vibration mode is important as it is the main driving source to actuate fluid in this groove type channel.

Figure 4(c) and (d) shows the fluid flow inside the groove type microchannel of width 50 μm and 280 μm, respectively, under 50 times magnification. Fluorescent microspheres (BioScientific, Gymea NSW) of diameter 1 μm were used to visualize the type of induced flow and the fluid motion was recorded using a high speed video camera (MotionBLITZ HSC-kit, Mikrotron, Germany) recording at the speed of 500 frames per second. The flow velocities inside the 50 μm groove type channel appeared to be constant cross the channel width, whereas vortices were observed as the channel width increased to 280 μm. This finding is consistent with our prediction and thus our model is verified.

4 Conclusions

A promising scheme for new SAW driven microchannel flow has been outlined, from the concept to the fabrication and preliminary experimental results. The experimental results show that SAW driven flow in a microchannel without vortices is possible. Significant advantages of using SAW streaming is the high body force actuation and the simplification to fabricate the devices. Flow velocities in the order of 10^0 mm/s were observed in the initial trial. The numerical results agreed with the experimental results.

References

[1] R. M. White and F. W. Voltmer. Direct piezoelectric coupling to surface elastic waves, Applied Physics Letters, 7 (1965) 314-316.

[2] T. Uchida, T. Suzuki and S. Shiokawa, Investigation of acoustic streaming excited by surface acoustic waves, 1995 IEEE Ultrasonics Symposium, 1995, pp. 1081-1084.

[3] Sir J. Lighthill, Acoustic streaming, *Journal of Sound and Vibration*, 61 (1978) 391-418.

[4] K. Chono, N. Shimizu, Y. Matsui, J. Kondoh and S. Shiokawa, Development of noval atomozation system based on SAW streaming, *Japanese Journal of Applied Physics*, 43 (2004) 2987-2991.

[5] A. Wixforth. Acoustically driven planar microfluidics, Superlattices and Microstructures, 33 (2003) 389-396.

[6] C. J. Strobl, Z. v. Guttenberg and A. Wixforth. Nano- and pico-dispensing of fluids on planar substrates using SAW, IEEE Transaction on Ultrasonics, Ferroelectrics and Frequency Control, 51 (2004) 1432-1436.

[7] A. Renaudin, P. Tabourier, V. Zhang, J. C. Camart and C. Druon. SAW nanopump for handling droplets in view of biological applications, Sensors and Actuators B, 113 (2006) 389-397.

[8] W. K. Tseng, J. L. Lin, W. C. Sung, S. H. Chen, and G. B. Lee. Active micro-mixers using surface acoustic waves on Y-cut 128^0 $LiNbO_3$, Journal of Micromechanics and Microengineering, 16 (2006) 539-548.

[9] K. Sritharan, C. J. Strobl, M. F. Schneider, A. Wixforth, and Z. Guttenberg. Acoustic mixing at low Reynold's numbers, Applied Physics Letters, 88 (2006) 054102.

[10] H. F. Tiersen. Wave propagation in an infinite piezoelectric plate. Journal of Acoustical Society of America, 35 (1963) 234-239.

[11] J. J. Campbell and W. R. Jones. A method for estimating optimal crystal cuts and propagation directions for excitation of piezoelectric surface waves. IEEE Transaction on Sonics and Ultrasonic, 15 (1968) 209-217.

[12] W. L. Nyborg. Acoustic streaming. San Diego: Academic Press Inc, 1965, 265-331.

[13] P. Morse and K. Ingard. Theoretical acoustics (MacGraw-Hill. 1968).

[14] C. E. Bradley. Acoustic streaming field structure: the influence of the radiator. Journal of Aco ustical Society of America , 100 (1996) 1399-1408.